Supplementary Information for
Collective spin reorientation-triggered large hysteresis-free magnetostriction with high strain sensitivity in $TbMn_6Sn_6$

Jie Du,[1,ⱡ] Liang Yao,[1,ⱡ] Xiaodong Zhou,[2,*] Cunlong Dong,[3] Yuming Gai,[1,3] Hang Li,[1] Yuan Yao,[3] Xuekui Xi,[3] Yong-Chang Lau,[3] Guoqiang Yu,[3] Wenhong Wang[1,2*]

[1] Institute of Quantum Materials and Devices; School of Electronics and Information Engineering, Tiangong University, Tianjin 300387, China

[2]School of Physical Science and Technology, Tiangong University, Tianjin 300387, China

[3] Beijing National Laboratory for Condensed Matter Physics, Institute of Physics, Chinese Academy of Sciences, Beijing, China.

ⱡThese authors contributed equally to this work.

* Corresponding author: zhouxiaodong@tiangong.edu.cn;

wenhongwang@tiangong.edu.cn

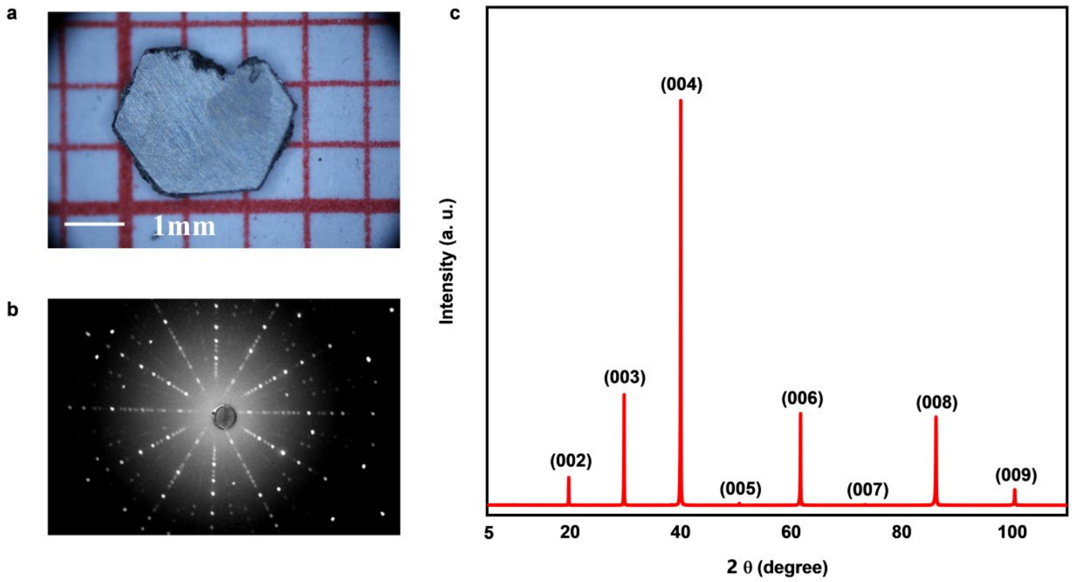

Figure S1 | Structural characterization of $TbMn_6Sn_6$ single crystals. a Optical image of a $TbMn_6Sn_6$ single crystal with a typical plate-like morphology. b Laue diffraction pattern of the $TbMn_6Sn_6$ single crystal, confirming the single-crystalline nature and determining the in-plane crystallographic orientation. c Room-temperature X-ray diffraction (XRD) pattern collected from the crystal surface, showing only the (00l) reflections, indicating the high crystallinity and preferred orientation along the crystallographic *c*-axis.

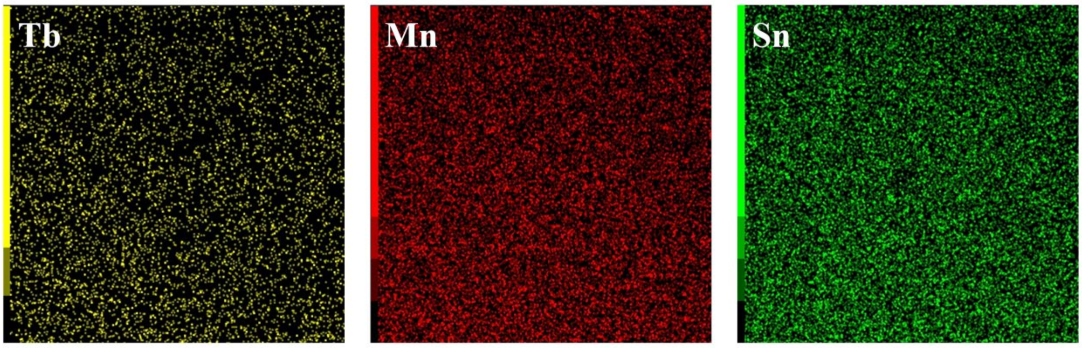

Figure S2 | Energy-dispersive X-ray spectroscopy elemental mapping of Tb, Mn, and Sn, demonstrating high chemical homogeneity.

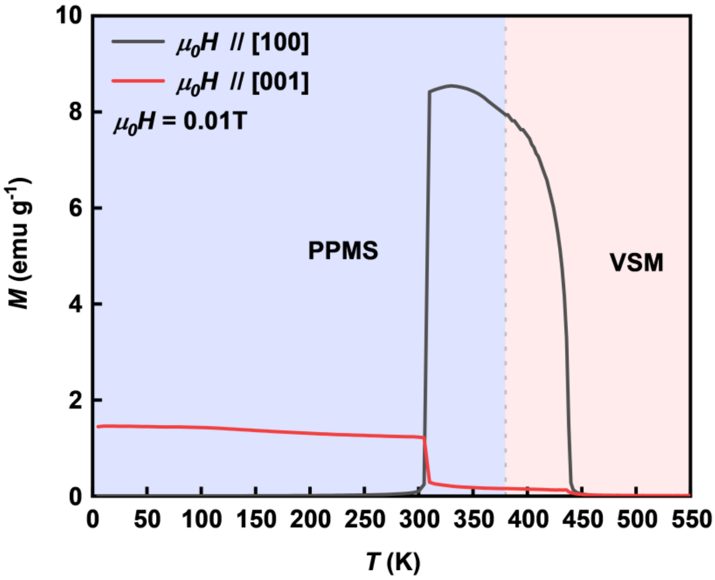

Figure S3 | Temperature-dependent magnetization of $TbMn_6Sn_6$ measured by PPMS (T≤380K) and VSM (T≥380K), respectively. Temperature-dependent magnetization curves measured under $\mu_0 H = 0.01\ T$ with the magnetic field applied along the [100] and [001] directions, combining PPMS and VSM measurements to cover the full temperature range.

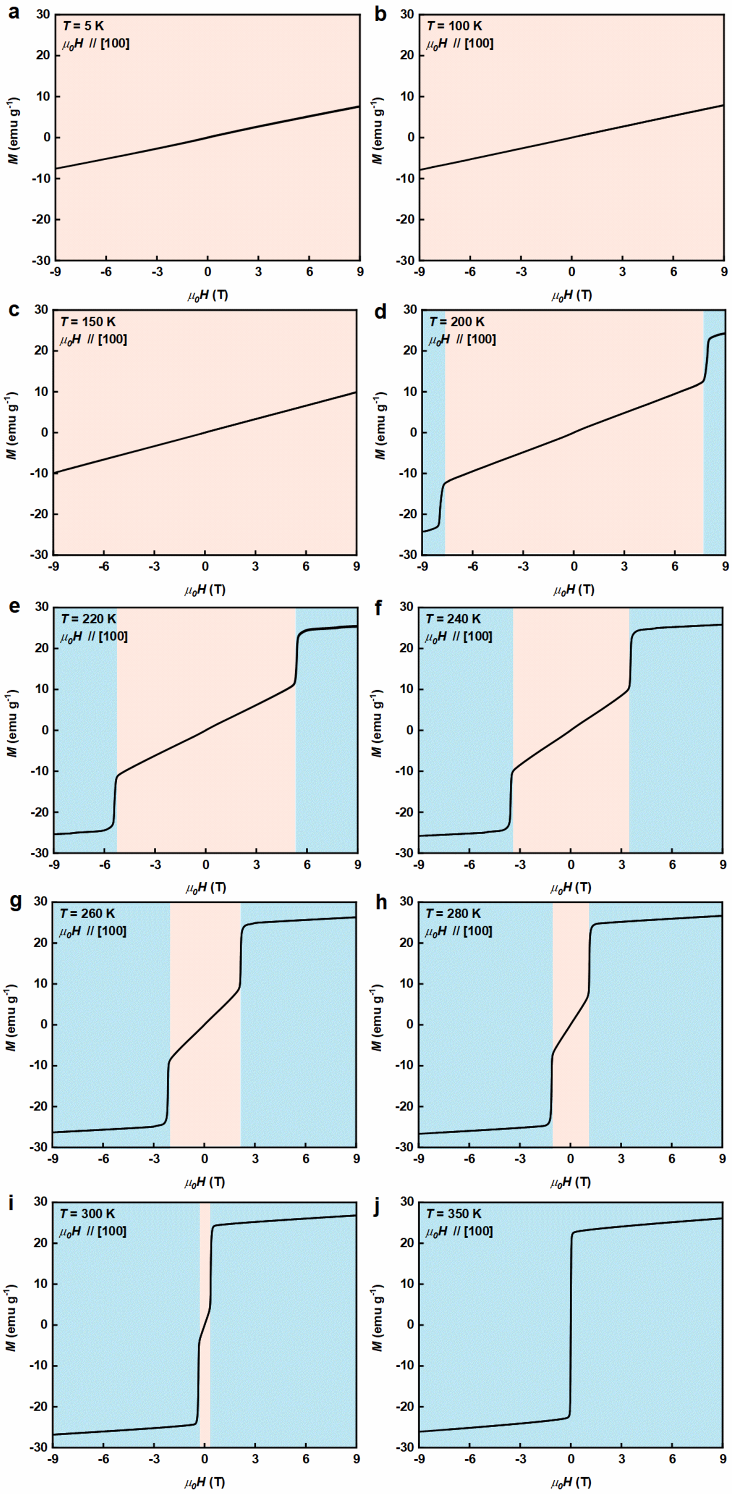

Figure S4 | Temperature evolution of the field-induced SR transition in $TbMn_6Sn_6$. a-j, Temperature-dependent *M-H* curves of $TbMn_6Sn_6$ measured with *H* // [100]. The progressive evolution of the magnetization curves with temperature illustrates the shift of the SR transition region and provides the characteristic fields (H_1 and H_2) used to construct the magnetic phase diagram.

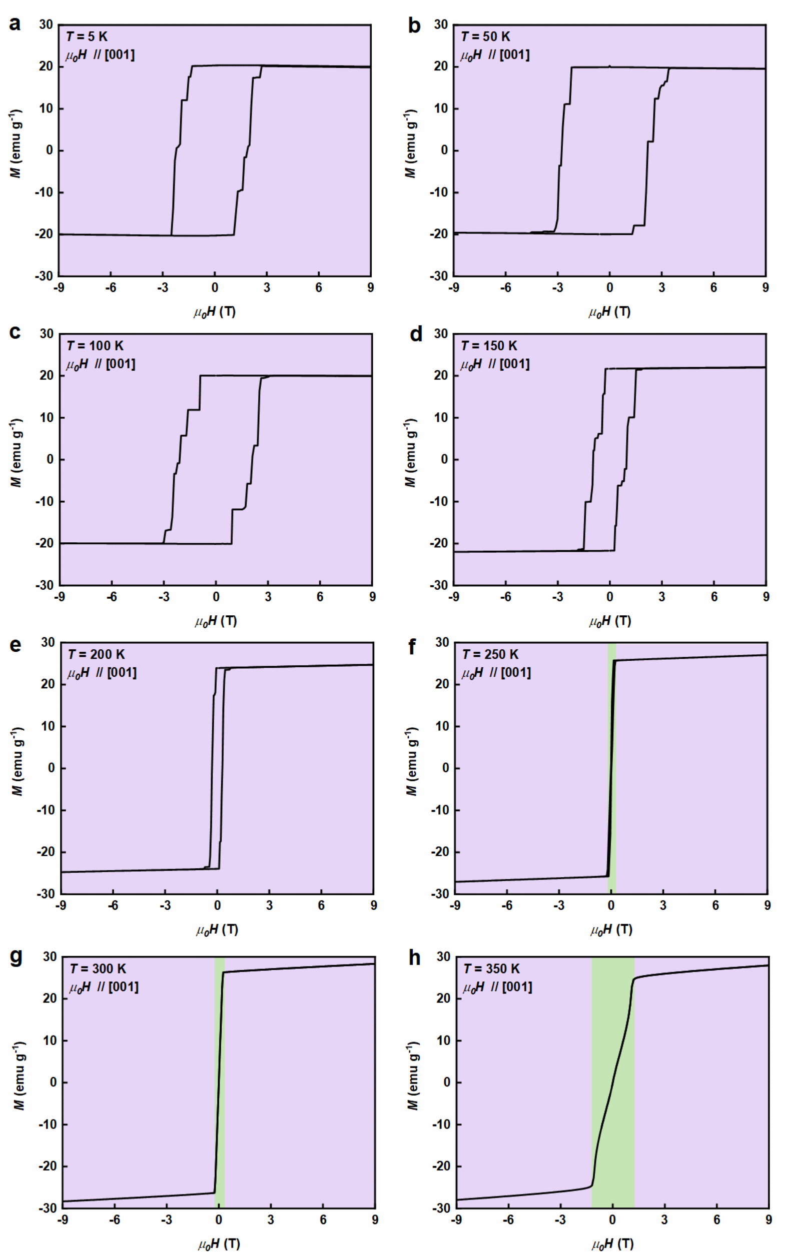

Figure S5 | Temperature evolution of magnetic anisotropy in $TbMn_6Sn_6$. a-h, Temperature-dependent *M*-*H* curves of $TbMn_6Sn_6$ measured with *H* // [001]. The magnetic-field-dependent evolution of magnetization reveals the temperature-dependent magnetic anisotropy and the evolution of the ferrimagnetic state along the out-of-plane direction.

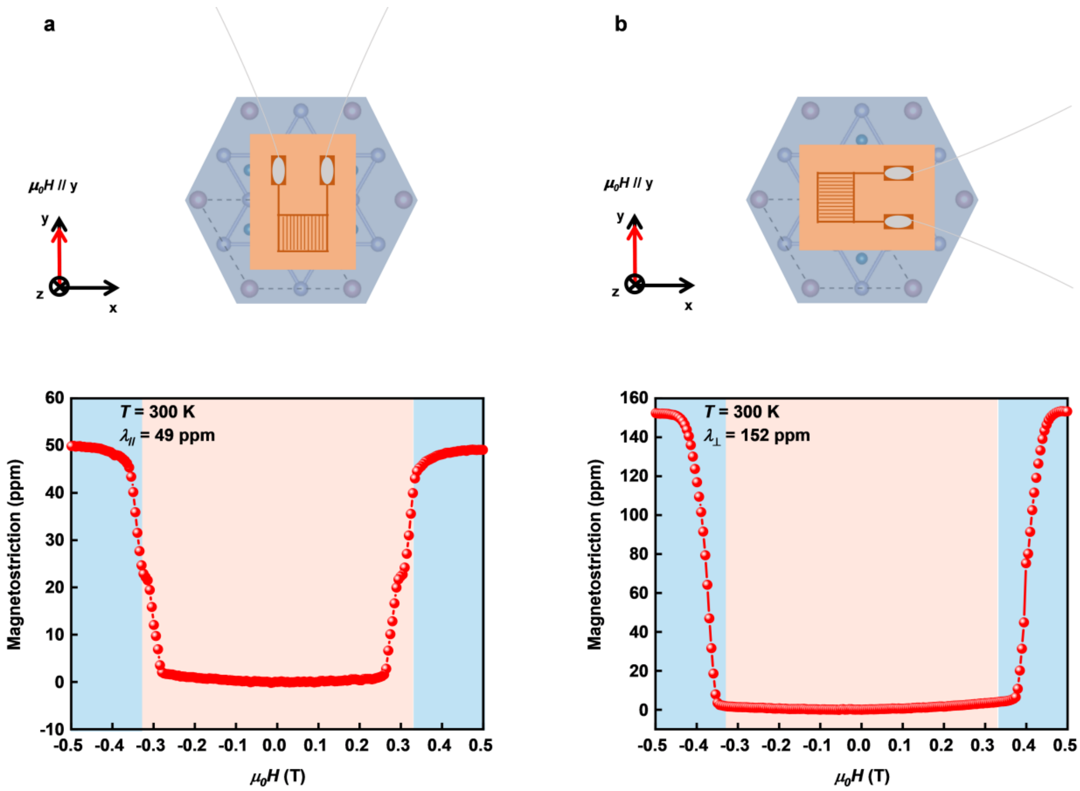

Figure S6 | Transition-enabled large anisotropic magnetostriction in $TbMn_6Sn_6$. a Longitudinal magnetostriction ($\lambda_{//}$) measured with the magnetic field applied along the [120] direction at room temperature. b Transverse magnetostriction ($\lambda_{\perp}$) measured perpendicular to the applied magnetic field, showing the enhanced strain response across the field-induced SR transition.

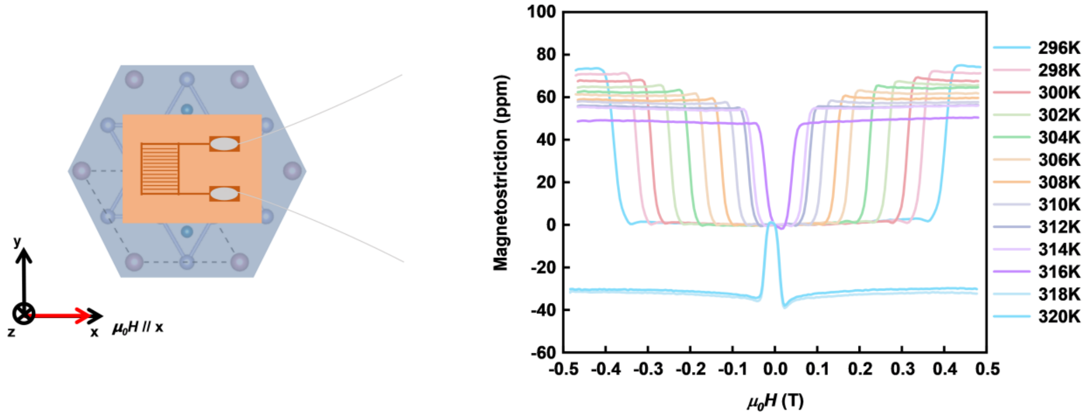

Figure S7 | Temperature-dependent longitudinal magnetostriction measured at selected temperatures across the SR transition regime.

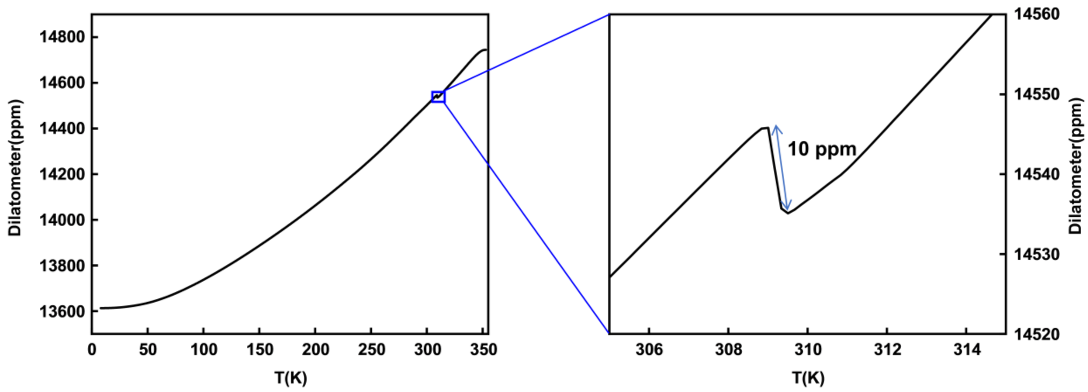

Figure S8 | Temperature-dependent strain variation of $TbMn_6Sn_6$ in zero magnetic field. Temperature-dependent strain evolution of $TbMn_6Sn_6$ measured without an external magnetic field. The strain variation across the SR transition region is limited compared with the field-induced magnetostrictive response, indicating that the giant magnetostriction originates from magnetic-field-driven reconstruction rather than temperature-induced lattice deformation.

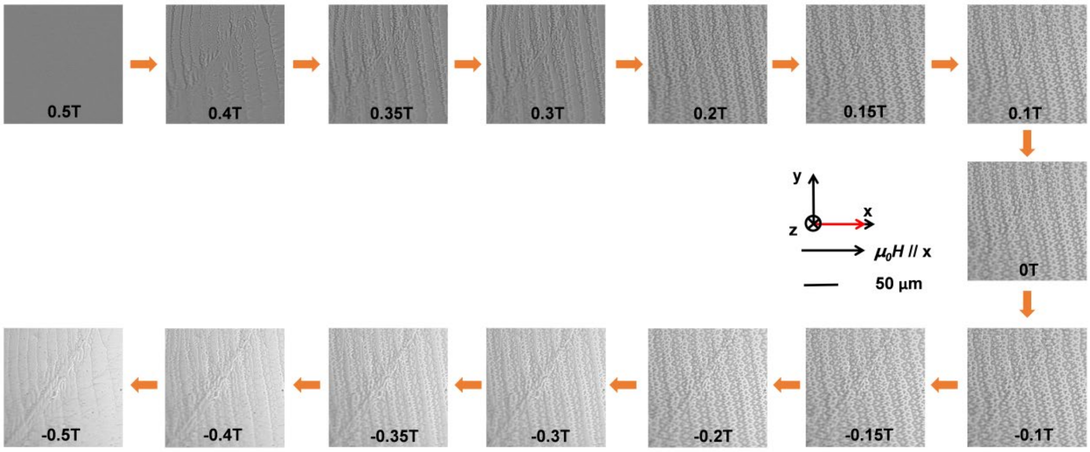

Figure S9 | Reversible magnetic-domain reconstruction under magnetic-field reversal in $TbMn_6Sn_6$. Sequential MOKE images recorded during an in-plane magnetic-field sweep from +0.5 T to −0.5 T. The stripe-domain configuration evolves continuously with decreasing magnetic field and undergoes reversible reconstruction during the field reversal process, reflecting the field-driven evolution of the magnetic state across the SR transition.

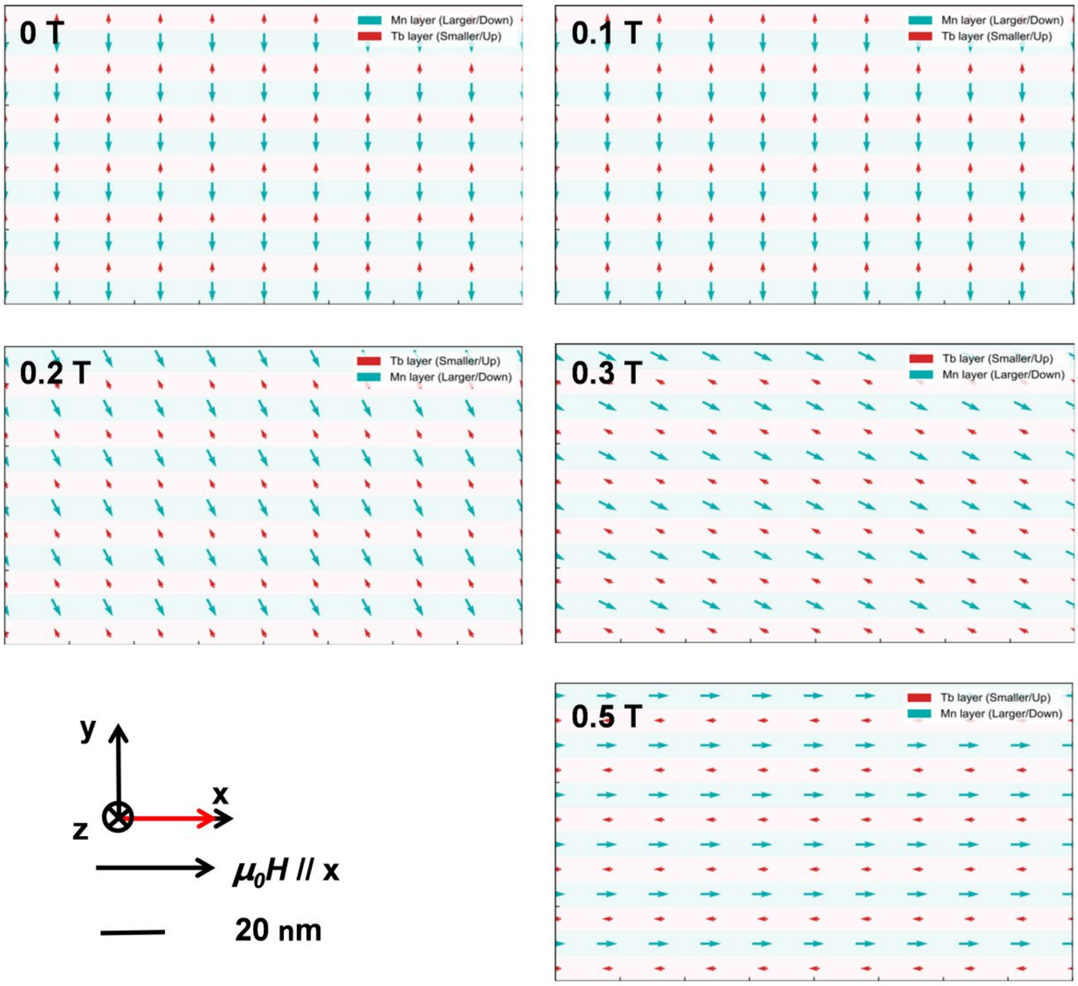

Figure S10 | Micromagnetic simulation of field-induced collective spin rotation in $TbMn_6Sn_6$. Field-dependent spin configurations obtained from OOMMF simulations of a 200 nm thick $TbMn_6Sn_6$ model under an in-plane magnetic field. As the magnetic field increases from 0 to 0.5 T, the Tb and Mn magnetic moments rotate collectively toward the field direction while maintaining their antiparallel alignment, demonstrating the preservation of the Tb-Mn ferrimagnetic coupling during the field-induced SR process.

Table SI | Comparison of magnetostrictive strain sensitivities in representative materials.

material	T	H_1	H_2	Magnetostriction	$\lvert\Delta\lambda/\Delta H\rvert$ (ppm/Oe)
Mn_3Sn[1]	**300 K**	**0 T**	**1 T**	**0-41.6 ppm**	**0.00416**
MnTe[2]	**50 K**	**0 T**	**0.7 T**	**0-32 ppm**	**0.004571**
$Fe_{35}Co_{35}Al_{10}Cr_{10}Ni_{10}$[3]	**300 K**	**1 T**	**2.5 T**	**50-200 ppm**	**0.01**
YMn_6Sn_6	**120 K**	**5.11 T**	**5.9 T**	**(-376)-(-495)ppm**	**0.015**
Ni[4]	**300 K**	**0.75 T**	**1 T**	**1-(-10) ppm**	**0.044**
FeCo[5]	**300 K**	**0.025 T**	**0.1 T**	**5-100 ppm**	**0.128**
Fe[6]	**300 K**	**0.007 T**	**0.012 T**	**4-13 ppm**	**0.18**
Co[6]	**300 K**	**0 T**	**0.01 T**	**0-20 ppm**	**0.2**
$Tb_{0.27}Dy_{0.73}Fe_{1.95}$[7]	**300 K**	**0.05 T**	**0.12 T**	**0-200 ppm**	**0.32**
$SmFe_2$[8]	**300 K**	**0 T**	**0.25 T**	**0-950 ppm**	**0.38**
$Fe_{81}Ga_{19}$[9]	**300 K**	**0.05 T**	**0.09 T**	**50-250 ppm**	**0.5**
Ho[10]	**45 K**	**1 T**	**1.6 T**	**100-3600 ppm**	**0.58**
Dy[10]	**20 K**	**0 T**	**0.5 T**	**0-4500 ppm**	**0.9**
$Fe_{67.7}Pd_{32.3}$[11]	**120 K**	**0 T**	**0.08 T**	**0-800 ppm**	**1**
$TbMn_6Sn_6$ (This work)	**300 K**	**0.346 T**	**0.378 T**	**6.4-142 ppm**	**0.42**
$TbMn_6Sn_6$ (This work)	**310 K**	**0.0098T**	**0.0308T**	**17-143 ppm**	**0.6**

References:

1. X. Wang, W. Dong, P. Qin, et al., “Giant Non-saturating Exchange Striction in a Noncollinear Antiferromagnet,” *Advanced Materials 37*, no. 18 (2025): 2500829, https://doi.org/10.1002/adma.202500829.

2. Z. Duan, Q. Xu, P. Qin, et al., “Saturated and Anisotropic Magnetostriction in an Altermagnet,” *Journal of the American Chemical Society* (2026): jacs.6c02730, https://doi.org/10.1021/jacs.6c02730.

3. J. Gou, Y. Pan, T. Yang, et al., “Large Nonhysteretic Volume Magnetostriction in a Strong and Ductile High-entropy Alloy,” *Advanced Materials 36*, no. 35 (2024): 2404192, https://doi.org/10.1002/adma.202404192.

4. E. Arakawa, N. Aizawa, Y. Park, and J.-Y. Choi, “Magnetostriction of a Single Crystal of Nickel Observed with an X-Ray Four-Circle Goniometer,” *Journal of Physics and Chemistry of Solids 68*, no. 11 (2007): 2138–2142, https://doi.org/10.1016/j.jpcs.2007.08.017.

5. Z. Wang, K. Mori, K. Nakajima, and F. Narita, “Fabrication, Modeling and Characterization of Magnetostrictive Short Fiber Composites,” *Materials 13*, no. 7 (2020): 1494, https://doi.org/10.3390/ma13071494.

6. P. McCorkle, “Magnetostriction and Magnetoelectric Effects in Iron, Nickel and Cobalt,” *Physical Review 22*, no. 3 (1923): 271–278, https://doi.org/10.1103/PhysRev.22.271.

7. Z. Yang, J. Li, Z. Zhou, J. Gong, X. Bao, and X. Gao, “Recent Advances in Magnetostrictive Tb-Dy-Fe Alloys,” *Metals 12*, no. 2 (2022): 341, https://doi.org/10.3390/met12020341.

8. Y. Wang, W. J. Ren, Y. H. Yang, B. Li, J. Li, and Z. D. Zhang, “Magnetostrictive Properties of the

Heavy-Rare-Earth-Free $Sm_{1-x}Nd_xFe_2$ Compounds," *Journal of Applied Physics 113*, no. 14 (2013): 143903, https://doi.org/10.1063/1.4801340.
9. B. Qiao, S. Zhao, J. Yao, et al., "Highly Stable Magnetostriction in Nanoheterogeneous Fe_{81} Ga_{19} Alloy Enabled by Uncoarsening of Nanoprecipitates Due to Negative Interfacial Energy," *Advanced Functional Materials 35*, no. 17 (2025): 2419157, https://doi.org/10.1002/adfm.202419157.
10. S. Legvold, J. Alstad, and J. Rhyne, "Giant Magnetostriction in Dysprosium and Holmium Single Crystals," *Physical Review Letters 10*, no. 12 (1963): 509–511, https://doi.org/10.1103/PhysRevLett.10.509.
11. S. Ren, D. Xue, Y. Ji, X. Liu, S. Yang, and X. Ren, "Low-Field-Triggered Large Magnetostriction in Iron-Palladium Strain Glass Alloys," *Physical Review Letters 119*, no. 12 (2017): 125701, https://doi.org/10.1103/PhysRevLett.119.125701.